^{7}Li NMR and Two-Dimensional Exchange Study of Lithium Dynamics in Monoclinic $Li_3V_2(PO_4)_3$

L. S. Cahill, R. P. Chapman, J. F. Britten, and G. R. Goward*

Department of Chemistry and Brockhouse Institute for Materials Research, McMaster University, 1280 Main Street W., Hamilton, ON, L8S 4M1 Canada

Received: December 2, 2005; In Final Form: January 26, 2006

High-resolution solid-state ^{7}Li NMR was used to characterize the structure and dynamics of lithium ion transport in monoclinic $Li_3V_2(PO_4)_3$. Under fast magic-angle spinning (MAS) conditions (25 kHz), three resonances are clearly resolved and assigned to the three unique crystallographic sites. This assignment is based on the Fermi-contact delocalization interaction between the unpaired d-electrons at the vanadium centers and the lithium ions. One-dimensional variable-temperature NMR and two-dimensional exchange spectroscopy (EXSY) are used to probe Li mobility between the three sites. Very fast exchange, on the microsecond time scale, was observed for the Li hopping processes. Activation energies are determined and correlated to structural properties including interatomic Li distances and Li−O bottleneck sizes.

Introduction

The high energy density and long lifetime of lithium ion batteries are responsible for their dominance in the field of portable energy sources.[1] Currently, much research is focused on the basic components of the lithium ion cell to obtain enhanced performance. Investigations of the cathode material strive to improve upon the current standard, $LiCoO_2$, which suffers from slow cycling and the high cost and toxicity of cobalt. A material that has recently attracted interest as a potential cathode material is lithium vanadium phosphate, $Li_3V_2(PO_4)_3$. It crystallizes in a structure similar to the open framework NASICON (a family of Na superionic conductors) with corner-shared VO_6 octahedra and PO_4^{2-} tetrahedra.[2,3] Lithium metal phosphates have high, but operative, redox potentials coupled with good electrochemical and thermal stability.[4] They also have exceptional ionic conductivity resulting from the large interstitial space created by the PO_4^{2-} units, allowing for fast ion migration in three dimensions. $Li_3V_2(PO_4)_3$ exhibits a theoretical capacity of 197 (mA h)/g, the highest of the phosphates.[5] Recently, it has been shown that all three lithium sites can be reversibly extracted from the lattice, resulting in a capacity approaching the theoretical value.[6,7] Coating the particles with a conductive carbon matrix has addressed the concerns about electronic conductivity and has allowed full access to this capacity.[6]

$Li_3V_2(PO_4)_3$ exists in two different forms: a rhombohedral phase and the thermodynamically stable monoclinic phase, α-$Li_3V_2(PO_4)_3$, with symmetry $P2_1/n$. The latter has a closer packing but has been shown to possess better electrochemical properties.[8] Monoclinic $Li_3V_2(PO_4)_3$ undergoes several two-phase transitions between 3.0 and 4.7 V versus Li^+/Li but retains electrochemical reversibility, forming a solid solution upon lithium reinsertion.[6,9] Despite all of the phase changes, it has been shown by neutron diffraction to avoid undergoing large structural changes upon cycling.[10] The ability of lithium ions to be transported is crucial to achieving high cell performance and reversible capacity and depends on the electronic and structural properties of the material. An understanding of the microscopic mobility of the lithium ions, both preferred paths and hopping rates, is essential to explaining the macroscopic electrochemical behavior as well as for improving the performance of these promising cathode materials.

Solid-state nuclear magnetic resonance (NMR) is a powerful tool for elucidation of local structure and dynamics. Rhombohedral $Li_3V_2(PO_4)_3$ has been studied using solid-state ^{7}Li NMR and shown to have a single resonance at 85 ppm.[11] The monoclinic form has three crystallographically unique lithium sites which have distinctly different chemical shifts, attributed to the Fermi-contact interaction—the transfer of electron spin density from the V^{3+} t_{2g} orbitals to the Li 2s orbitals.[12] Previous NMR studies have shown changes in the ^{7}Li isotropic chemical shifts upon deinsertion/insertion using chemical oxidation and reduction methods.[12,13]

The investigation of exchange processes between ions on multiple sites can be accomplished using two-dimensional exchange NMR spectroscopy (2D EXSY).[14] This has been demonstrated in studies of lithium transport in Li_4SiO_4[15] and in pristine $LiMn_2O_4$.[16] 2D EXSY has also been used to probe mobility in fluoride-ion conductors such as α-PbF_2 and $BaSnF_4$.[17,18] Recent studies have demonstrated the use of ^{17}O and ^{6}Li 2D EXSY to study ion motion in conductors Bi_2WO_6 and Li_7MnN_4, respectively.[19,20]

Here, we investigate lithium dynamics in monoclinic $Li_3V_2(PO_4)_3$ through variable-temperature ^{7}Li magic-angle spinning (MAS) NMR spectra and exchange-based solid-state NMR studies. The latter technique provides information about the mechanism of lithium hopping in $Li_3V_2(PO_4)_3$, which sites are active, and the time scale of the processes. These measurements allow calculation of activation energies, which are correlated directly to interatomic Li−Li distances. Moreover, the diffusion rates are correlated to a bottleneck, identified through the minimum in the ion-framework contact along the lithium ion pathway. These results are compared to related works based on impedance spectroscopy measurements for rhombohedral NASICON materials.[21−23]

* Corresponding author. E-mail: goward@mcmaster.ca. Phone: (905)-525-9140 × 24176. Fax: (905)-522-2509.

10.1021/jp057015+ CCC: $33.50
Published on Web 03/17/2006

Experimental Section

Sample Preparation. $Li_3V_2(PO_4)_3$ was prepared by mixing stoichiometric amounts of Li_2CO_3 (Aldrich, 99+%), V_2O_5 (Aldrich, 98+%), and $NH_4H_2PO_4$ (Alfa Aesar, 99.6%) as described by Adamson.[7] The mixture was heated to 300 °C for 3 h in air, ground, pelletized, and heated to 650 °C in a sealed tube furnace under a stream of pure hydrogen for 8 h. The Li-6 enriched sample was prepared using 50 wt % of $^6Li_2CO_3$ (Aldrich, 95 at. %). The synthesized samples were analyzed by powder X-ray diffraction using a Bruker D8 Advance powder diffractometer with Cu Kα radiation ($\lambda = 1.5406$ Å). Data were collected from 10 to 90° in 2θ at a step size of 0.023° and a step time of 13 s. The reflections match those detailed in the literature.[7,24]

Solid-State NMR. ^{7}Li MAS NMR spectra were acquired at a Larmor frequency of 116.6 MHz on a Bruker AV-300 spectrometer. The experiments were performed at low field to minimize the paramagnetic broadening.[25] A double-resonance probe supporting rotors of 2.5 mm in outer diameter was used with a spinning frequency of up to 25 kHz. The spectra are referenced to 1 M LiCl (aq) (0 ppm). ^{7}Li NMR spectra were acquired using a 90° pulse length of 3 μs and a recycle delay of 50 ms. The temperature was calibrated using $Sm_2Sn_2O_7$ as a shift thermometer.[26] The method for determining the temperature calibration is described in detail in a previous report.[27]

Spin-lattice relaxation times (T_1) were determined using a standard inversion recovery sequence. 2D exchange spectra were acquired using mixing times between 1 μs and 18 ms. The number of slices in the indirect dimension was 128, with 400 transients averaged per slice. Phase-sensitive detection in t_1 was achieved through the use of States-TPPI.

Results and Discussion

The three different lithium ion sites in the monoclinic $Li_3V_2(PO_4)_3$ lattice are at the general Wyckoff positions 4e, depicted in Figure 1a. The sites are well resolved by ^{7}Li NMR under fast MAS conditions of 25 kHz at resonance frequencies of 103, 52, and 17 ppm (site C, B, and A, respectively), seen in Figure 1b. Lithium B resides in a tetrahedral site while A and C are distorted trigonal bipyramids, with a long fifth Li−O bond.[13,28] Previous reports have been unable to correlate the chemical shifts directly to the crystallographic positions of the lithium ions. The full assignment is provided here, based on concepts which have been recently developed for the transfer of electron density through geometry-dependent polarization or delocalization mechanisms.[29] The magnitude of the observed NMR shifts in $Li_3V_2(PO_4)_3$ depends on the transfer of electron density from the paramagnetic V^{3+} ions through intervening oxygen atoms. These hyperfine shifts therefore depend on the number of paramagnetic cations within the Li coordination environment and the Li−O−V bond lengths and angles. On the basis of the crystal structure details found in the supporting information of ref 24, the Li−V distances and Li−O−V bond angles were determined using the Bruker SHELXTL version 6.14 program and are summarized in Table 1. Only the vanadium centers that are within the second coordination sphere of the lithium ions are considered able to donate electron density via the hyperfine coupling mechanism. This is due to the through-bond, rather than through-space, nature of the interaction. Differences in the local environments of the three sites, as detailed in Table 1 and illustrated in Figure 2, provide the basis for the chemical shift assignment.

The V^{3+} ions in $Li_3V_2(PO_4)_3$ are all in octahedral coordination environments, having partially occupied t_{2g} orbitals and empty e_g orbitals. As described for the case of octahedral-coordinated manganese ions in manganese oxides, there are two possible interactions for transferring electron density: delocalization and polarization.[29,30] The delocalization mechanism transfers electron density through direct M−O−Li orbital overlap with the singly occupied metal orbital. This always results in a positive spin transfer from the metal orbitals to the Li 2s orbital, moving the chemical shift toward higher frequency. Polarization results from the unpaired electrons polarizing doubly occupied orbitals, transferring negative electron density to the Li 2s orbital, and

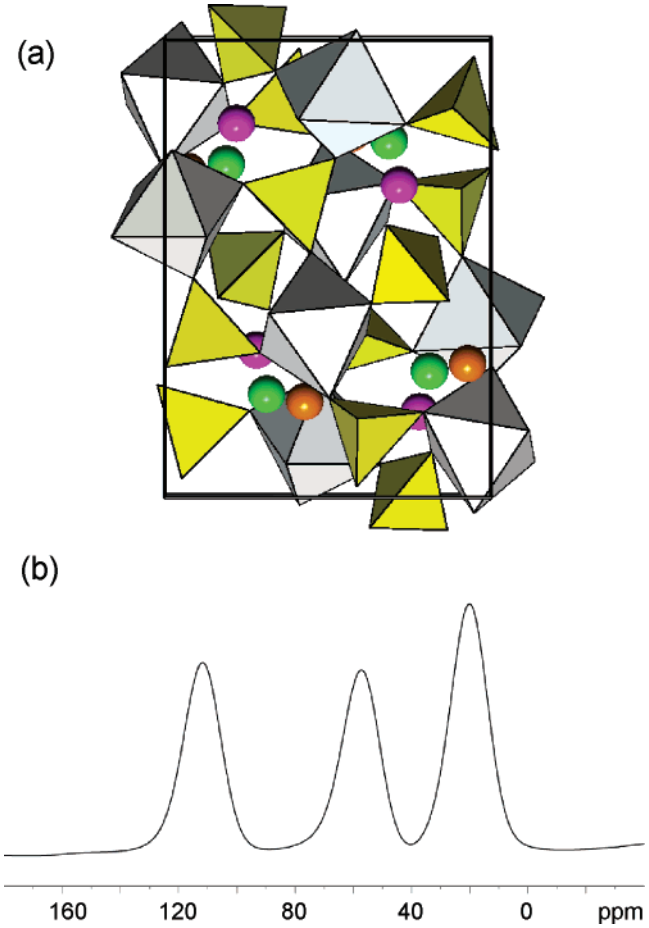

Figure 1. (a) Structure of $Li_3V_2(PO_4)_3$ along the *a* axis, showing the three unique Li ions A, B, and C in orange, purple, and green, respectively. The V−O octahedra are shown in gray, and the P−O tetrahedra are shown in yellow. (b) ^{7}Li MAS NMR spectrum acquired under ambient bearing gas temperature at 25 kHz. The three resonances, from lowest to highest frequency, correspond to sites A, B, and C.

TABLE 1: Local Environments for the Three Unique Li Sites as Defined by the Values of Li−O−V Angles and Li−V Bond Lengths

	Li−O−V angles (deg)	Li−V distances (Å)
A	88.4	2.70
	79.1	2.70
	74.9	2.70
	96.0	3.03
	99.7	3.03
B	94.5	2.93
	95.6	2.93
	99.4	2.97
	93.6	2.97
C	73.1	2.89
	87.9	2.89
	87.8	2.89
	106.6	3.33
	130.5	3.59

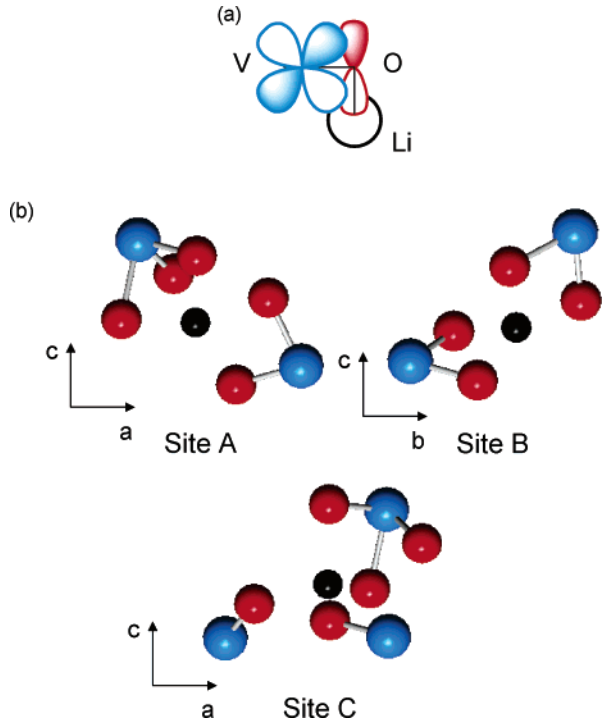

Figure 2. (a) Diagram representing how spin density is transferred via an ideal 90° Li−O−V^{3+} interaction. The orbitals overlap to transfer positive spin density by the delocalization mechanism from the V^{3+} t_{2g} orbital to the Li 2s nucleus via the intervening O 2p orbital. (b) Lithium coordination environments in monoclinic $Li_3V_2(PO_4)_3$. The vanadium centers depicted are found in the second coordination sphere and are responsible for donating positive spin density to the Li nucleus. The lithium atoms are shown in black, oxygen atoms, in red, and vanadium, in blue.

moving the chemical shift to lower frequency. Both mechanisms are geometry dependent, with the most efficient transfer occurring for the ideal 90° and 180° arrangements. The total transfer of electron density that each paramagnetic cation contributes to the hyperfine shift is additive, and in general, the delocalization mechanism is larger than polarization.

In $Li_3V_2(PO_4)_3$, with V^{3+} electron configuration $t_{2g}^2e_g^0$, there are only two possible mechanisms for spin transfer.[29] A 90° interaction occurs via the delocalization mechanism and results in the transfer of positive electron density from the t_{2g} orbital, through an O 2p orbital to the Li 2s orbital while a 180° interaction transfers negative density via polarization.[29] The ideal 90° interaction is depicted in Figure 2a where positive electron density can be transferred due to the orbital overlap.[29] Figure 2b shows the Li coordination environments in $Li_3V_2(PO_4)_3$ based on the crystallographic data (see Table 1). There is no possibility for transfer of negative electron density via the polarization mechanism because a 180° Li−O−V geometry is not present. On the basis of the arrangement of the polyhedra and the additive effect of the Fermi-contact interactions, it is possible to correlate the NMR shifts with the crystallographic sites. Sites A and B each have two vanadium centers in their second coordination spheres. Site A has the lowest frequency shift because the Li−O−V bond angles deviate substantially from 90°, resulting in poor overlap to allow a through-bond transfer of electron density. Site B possesses Li−O−V bond angles that are much closer to 90° (in the range of 93.6−99.4°), which accounts for the larger positive chemical shift. The local environment of Site C has three different vanadium centers within the second coordination sphere, with the correct geometry to contribute electron density to the Li 2s orbital, resulting in

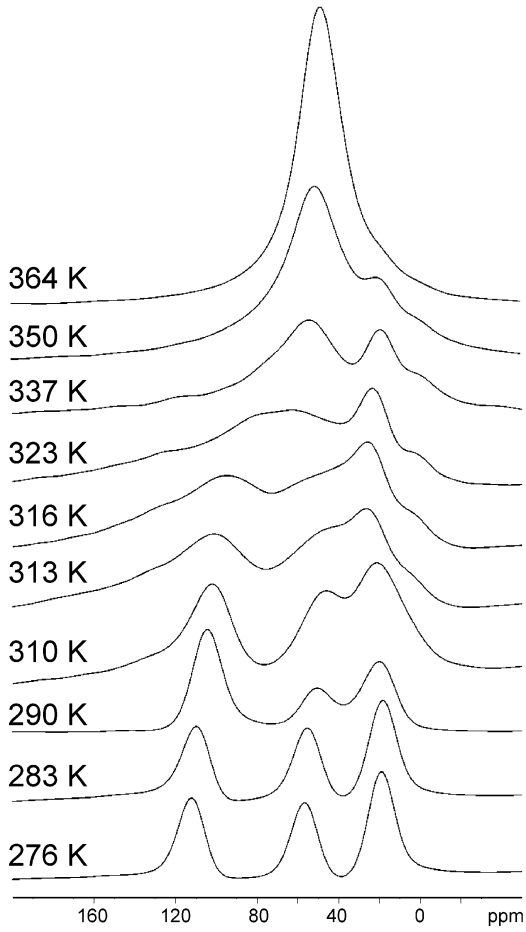

Figure 3. ^{7}Li MAS NMR variable-temperature spectra acquired at 25 kHz for $Li_3V_2(PO_4)_3$. The sample temperature is noted on each spectrum.

the shift observed at the highest frequency. This is the first unambiguous assignment of the hyperfine shifts in monoclinic $Li_3V_2(PO_4)_3$ to the crystallographic sites of the Li ions. This enables information obtained from ongoing NMR studies of electrochemically treated samples to be related to the local structure of $Li_3V_2(PO_4)_3$.

Figure 3 shows a one-dimensional (1D) variable-temperature study from 276 to 364 K, with the sample temperature corrected to include the heating effects of spinning at 25 kHz. The chemical shift has a linear dependence on temperature, showing Curie−Weiss behavior.[31] This rules out the possibility of contributions from diamagnetic and Van Vleck susceptibilities which both give rise to temperature-independent NMR shifts.[31] These materials are electronically insulating, and therefore, the possibility of a Knight shift can be ignored. The variable-temperature NMR measurements thereby confirm that the origin of the large chemical shifts is from hyperfine couplings of the Li nucleus with unpaired electron density, as described above. The intensity ratio of the three resonances, after performing spectral deconvolution of the full span of spinning sidebands, is approximately 1:1:1, as predicted from the crystal structure. Spin−lattice relaxation measurements (T_1) were performed, and all three resonances were found to have the same relaxation time of 6 ± 0.2 ms, which is extremely short due to relaxation induced by the paramagnetic V^{3+} ions. Determination of the T_1 values is essential because, in the EXSY experiment, mixing times longer than T_1 result in violation of the linear approximation of kinetics and the intensity of the cross peaks will decrease.[32] This is reflected in the EXSY pulse sequence where

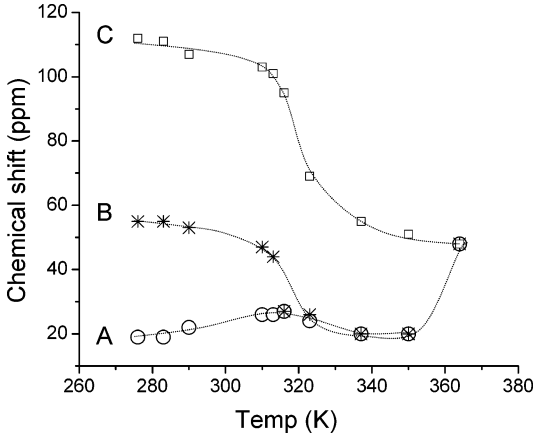

Figure 4. Plot of chemical shift (ppm) versus sample temperature (K) to illustrate the coalescence process from a 1D variable-temperature study for lithium sites A (circles), B (asterisks), and C (squares). The dotted lines are added as a guide for the eye and indicate that the chemical shift for resonance A and B trend toward each other until coalescence at 316 K. After this temperature, the three resonances coalesce to one average resonance at 364 K.

TABLE 2: Summary of Jump Frequencies and Correlation Times Estimated from 1D Variable-Temperature Spectra for $Li_3V_2(PO_4)_3$

	coalescence temp (K)	jump frequency (kHz)	correlation time, τ_c (μs)
AB	316	6.5	154
AC		21.0	47.7
BC		14.5	68.9

the second and third 90° pulses can be thought of as a saturation−recovery T_1 experiment. It is also important that all three resonances have similar T_1 values to ensure complete relaxation of the nuclear spins at all of the sites. In Figure 3, a small peak is visible at 0 ppm starting at 313 K. It has a long T_1 spin−lattice relaxation time, approximately 100 ms, consistent with a diamagnetic material such as Li_2CO_3 remaining from the synthesis. This resonance is present as a slight shoulder at lower temperatures but is not clearly visible because the line shape of the resonance at the lowest frequency is too broad.

It is clear that sites A and B coalesce first at and above 316 K, meaning that at this temperature these two sites are exchanging at a rate of $\pi\upsilon/\sqrt{2}$ comparable to the separation in Hz, υ, between the two resonances.[33] Figure 4, a plot of chemical shift versus sample temperature for each of the three resonances, illustrates the coalescence processes that occur in $Li_3V_2(PO_4)_3$ with increasing temperature. Resonances A and B shift toward each other, as identified by the initial shift of resonance B to lower chemical shift while A moves to higher chemical shift. These resonances appear to converge at 316 K, which corresponds to a jump frequency of higher than 6.5 kHz or a correlation time, τ_c, of 154 μs. Beyond this temperature, the AB resonance moves to higher frequency, coalescing with resonance C, which trends to lower frequency throughout the variable-temperature experiment. At 364 K, all three sites are exchanging faster than the NMR time scale and only one average resonance is observed. A summary of the jump frequencies and correlation times is given in Table 2. The correlation times provide a measure of the time scale for Li ion motion. The temperature for coalescence of sites AC and BC cannot be determined directly from the 1D variable-temperature study because the resonances corresponding to site A and B have already coalesced. It is clear, however, that all three sites experience motional averaging and that 2D experiments are necessary to study the exchange among the multiple sites. The 2D EXSY spectra were collected at low temperatures (276−290 K) because at room temperature ion exchange happens at a rate which causes substantial overlap of resonances A and B.

The direct exchange of multiple lithium sites can be observed as cross peaks in the 2D EXSY spectra. The rate of the exchange process is studied through the evolution of the cross peak intensity as a function of the mixing time, τ_{mix}. Figure 5a shows the 2D spectrum for $Li_3V_2(PO_4)_3$ collected at room temperature with a mixing time of 1 μs. There are only individual signals present along the diagonal, indicating that no exchange is taking place at this time scale. As the mixing time is increased to 50 μs (Figure 5b), clear cross peaks become evident between the B and C sites and are weakly evident between A and B. This result is mirrored in the variable-temperature study which also predicts a microsecond time scale for Li hopping. Figure 5c, at a mixing time of 500 μs, shows that cross peaks between all three sites are observed. A microsecond time scale for lithium hopping at room temperature in $Li_3V_2(PO_4)_3$ is determined by this qualitative analysis and by quantitative integrations of the cross peak intensities as a function of temperature (vida infra). This is much faster than the millisecond range seen for the Li ion jump rate in $LiMn_2O_4$.[16]

The transfer of magnetization between two sets of spins commonly occurs by two mechanisms: chemical exchange and spin diffusion. The latter process is a magnetization transfer through dipolar coupled spins, and its contribution to the exchange data was examined. To distinguish between chemical exchange and spin diffusion, the synthesis was performed with a mixture of 50% Li-6 enriched Li_2CO_3. This varied the extent of the homonuclear dipolar coupling between the ^{7}Li nuclei, but because no change in the cross peak intensity was observed, the contributions from spin diffusion can be considered negligible.[15] Moreover, the strongest ^{7}Li−^{7}Li dipolar coupling calculated for $Li_3V_2(PO_4)_3$ is approximately 600 Hz. This is much smaller than the typical values seen for ^{1}H where, for example, a CH_2 group has a dipolar coupling of 20 kHz.[34] A smaller magnetogyric ratio and longer interatomic distances account for the smaller ^{7}Li dipolar interactions. These dipolar couplings can be assumed to be removed with the fast MAS speeds used in this study. These factors confirm that the 2D EXSY approach is giving evidence for direct hopping of Li ions between different sites.

Figure 6 shows plots of relative intensity (cross peak intensity normalized to the sum of the intensities of the diagonal peaks) as a function of mixing time for all three sets of cross peaks at the three sampled temperatures. Increasing the mixing time results in increased cross peak intensity, reaching a saturation of the cross peaks at around 6 ms, consistent with the measured T_1 spin−lattice relaxation time. After this point, the cross peak intensity decreases due to violation of the linear approximation, as described earlier. Determination of the jump rate, k, between sites is done by fitting the buildup curves with a first-order exponential. By plotting ln k as a function of $1/T$ in an Arrhenius analysis, according to $\ln k = \ln A - E_a/RT$ and shown in Figure 7, the activation energies of the hopping processes between sites AB, AC, and BC are calculated to be 0.73, 0.79, and 0.83 eV respectively. The error estimates of the intensities are about 10%, based on multiple iterations of the spectral integration routine in the Bruker XwinNMR software, giving an error of about ±0.01 eV. The multiple iterations were performed on different spectra having the same experimental conditions and by changing the volume integrated on the same spectrum.

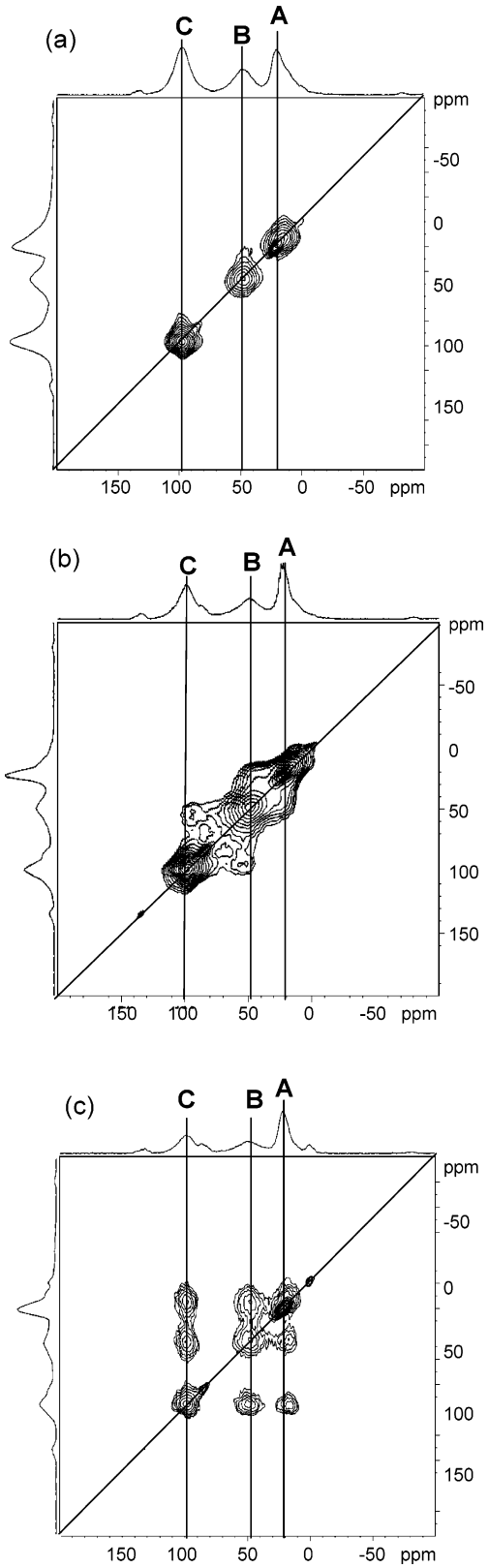

Figure 5. ^{7}Li EXSY spectra of $Li_3V_2(PO_4)_3$ acquired under ambient bearing gas temperature at 25 kHz with (a) $\tau_{mix} = 1$ μs; (b) $\tau_{mix} = 50$ μs; and (c) $\tau_{mix} = 500$ μs.

Ionic conductivity depends on the concentration of the ions of interest, their charge, and their mobility, $\sigma_i = c_i q \mu_i$.[35] The major factor controlling the ionic mobility is the activation energy, a representation of the ease of lithium hopping.[35] The values obtained for the activation energies of monoclinic $Li_3V_2(PO_4)_3$ are higher than those obtained from macroscopic

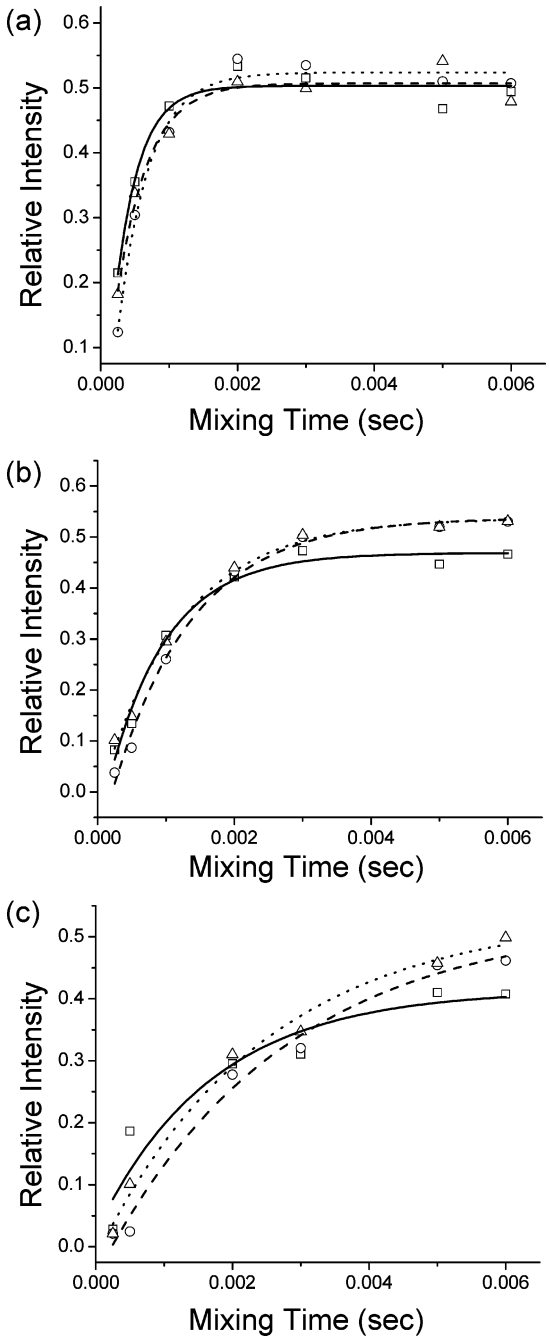

Figure 6. Relative intensity of the AB (squares), AC (circles), and BC (triangles) cross peaks as a function of mixing time (τ_{mix}) at (a) 276, (b) 283, and (c) 290 K. The first-order exponential fits are shown for cross peaks AB (solid line), AC (dashed line), and BC (dotted line).

ionic conductivity measurements for rhombohedral NASICON materials, ranging from 0.3 to 0.6 eV.[21−23] The interstitial space in the monoclinic phase of $Li_3V_2(PO_4)_3$ has a smaller free volume, so this result is not surprising since the openness of the conduction pathway is directly related to the ease of lithium ion mobility.[35] Another important factor in this difference is the relative occupancy of the lithium sites. The available activation energy data for the rhombohedral NASICON form is reported for partially occupied lithium sites.[21−23] Here, all three lithium sites are fully occupied. The lower number of vacancies for hopping requires a higher temperature dependence, reflected in the larger activation energies. Clearly, the microsecond time scale for exchange seen in the 2D EXSY experiments shows that the activation energies are not so large as to prevent fast motion of the lithium ions at room temperature.

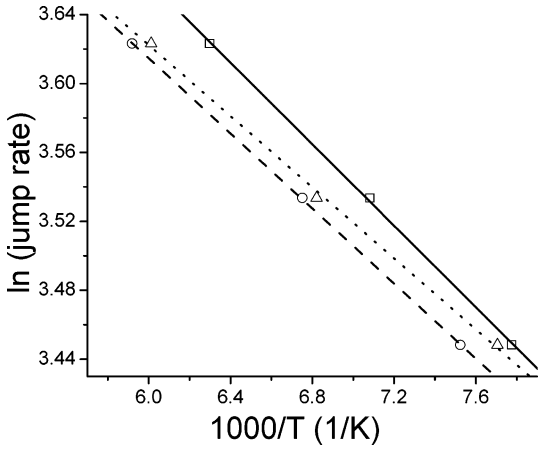

Figure 7. Arrhenius analysis to calculate activation energies. This plot shows ln(jump rate) versus 1000/*T* for cross peaks AB (solid line), AC (dashed line), and BC (dotted line).

TABLE 3: Summary of Activation Energies for Li Ion Hopping between Sites in $Li_3V_2(PO_4)_3$, Correlated to the Distances between the Two Sites and the Size of the Li−O Bottleneck within the Channel for Conduction

	activation energy (eV)	interatomic distances (Å)	Li−O bottleneck (Å)
AB	0.73 ± 0.01	3.08(3)	1.55
AC	0.79 ± 0.01	3.28(3)	1.44
BC	0.83 ± 0.01	3.43(3)	0.75

It is interesting to correlate the activation energies for lithium exchange to the electrochemical process. The relative ease of exchange is directly reflected in the sequential removal of lithium ions from the NASICON framework. Site A is removed at the lowest potential (i.e., requiring less energy), site B at an intermediate potential, and site C is removed at the highest potential, in other words, the most energetically costly.[13] Similarly, exchange occurs between sites AB at a faster rate than either of AC or BC. Moreover, the activation energies for the exchange processes follow the same sequence: AB at the lowest E_a value and BC at the highest. Since A is electrochemically extracted first, followed by B, and then C, the exchange partners are considered in the corresponding AB, AC, and BC pairings. The logical extension of this work will examine exchange partners and rates as a function of electrochemical cycling.

Here, we correlate activation energies to the known interatomic distances.[10] As summarized in Table 3, the activation energy increases as the distance between the lithium atoms increases. This finding is consistent with the activation energies determined by solid-state NMR since the further apart the sites are, the more energy required to jump between them. This relationship shows the ability of NMR as a local probe to be related to information obtained from long-range techniques such as X-ray diffraction. These activation energies directly identify molecular-level processes that may be necessary to facilitate long-range Li transport through the bulk cathode material.

The other factor which contributes to the ability of Li ions to hop from one site to another is the channel size. The presence of a bottleneck to diffusion, the narrowest point along the channels, has been investigated in several NASICON materials. Aranda et al. have correlated the activation energies determined by impedance analysis with the bottleneck size in several rhombohedral NASICON conductors where there are only two interstitial voids.[23,36] The bottleneck for the NASICON rhombohedral phase is determined from the hexagon formed by three MO_6 octahedral edges and three PO_4 tetrahedral edges.[2,36,37] The

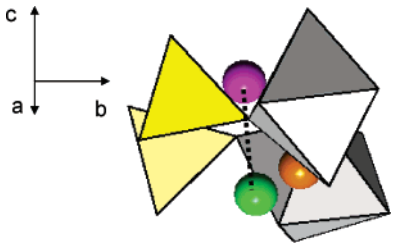

Figure 8. Diagram representing the pathway to diffusion for the Li sites B and C, in purple and green, respectively. The closest Li−O contact, determining the bottleneck to diffusion for sites B and C, was found with the oxygen involved in the top pair of corner-shared VO_6 and PO_4 units.

arrangement of the polyhedra in the monoclinic form is not oriented in a parallel fashion, so it is not possible to define the bottleneck area as a hexagonal surface. Using known atomic coordinates,[24] it is possible to model the monoclinic system using the Bruker SHELXTL program to visualize the environments along the channels in three dimensions. The Li ions have been shown to be distributed as sheets along the (a,c) plane.[10] The assumption is that conduction takes place in a straight line from Li site to Li site. A series of oxygen contacts along the pathway were determined as represented for hopping between sites B and C in Figure 8. The closest Li−O contact was used as a measure of the bottleneck. Summarized in Table 3, increasing activation energies are correlated to decreasing size of the bottleneck created by the closest oxygen ions, decreasing the ability of Li ions to jump readily. This validates the results and emphasizes the role of the channel size in Li ion diffusion. Thus, both interatomic Li distances and bottleneck sizes are important factors to consider for understanding ionic conductivity within metal phosphates and can be correlated to NMR observables.

Conclusion

2D ^{7}Li solid-state EXSY studies provide the first study of lithium dynamics in the monoclinic $Li_3V_2(PO_4)_3$ material. The mobility of the three lithium sites was found to occur on the microsecond time scale. The temperature dependence of the lithium ion hopping processes was determined in order to establish activation energies. These activation energies, ranging from 0.73 to 0.83 eV, were correlated directly to the interatomic Li−Li distances and to constraints or bottlenecks along the ion conduction pathways. $Li_3V_2(PO_4)_3$ has been shown to have commercial viability as a cathode material in lithium ion batteries, making it valuable to understand transport processes on the microscopic scale with regards to lithium ion hopping. The application of 2D EXSY NMR to characterize lithium dynamics in electrode materials can be extended to both electrochemically cycled materials and to other members of the lithium metal phosphate family.

Acknowledgment. The authors are grateful to L.F. Nazar and S.-C. Yin for helpful discussions regarding preparation of the $Li_3V_2(PO_4)_3$ and for providing an initial sample. We are also grateful to A.D. Bain and C.P. Grey for insightful comments. L.S.C. acknowledges scholarship support from NSERC. This research was supported through the NSERC Discovery Grant program.

References and Notes

(1) Tarascon, J. M.; Armand, M. *Nature* **2001**, *414*, 359.
(2) Hong, H. Y. P. *Mater. Res. Bull.* **1976**, *11*, 173.

(3) Goodenough, J. B.; Hong, H. Y. P.; Kafalas, J. A. *Mater. Res. Bull.* **1976**, *11*, 203.
(4) Nanjundaswamy, K. S.; Padhi, A. K.; Goodenough, J. B.; Okada, S.; Ohtsuka, H.; Arai, H.; Yamaki, J. *Solid State Ionics* **1996**, *92*, 1.
(5) Morgan, D.; Ceder, G.; Saidi, M. Y.; Barker, J.; Swoyer, J.; Huang, H.; Adamson, G. *Chem. Mater.* **2002**, *14*, 4684.
(6) Huang, H.; Yin, S. C.; Kerr, T.; Taylor, N.; Nazar, L. F. *Adv. Mater.* **2002**, *14*, 1525.
(7) Saidi, M. Y.; Barker, J.; Huang, H.; Swoyer, J. L.; Adamson, G. *Electrochem. Solid State Lett.* **2002**, *5*, A149.
(8) Ohkawa, H.; Yoshida, K.; Saito, M.; Uematsu, K.; Toda, K.; Sato, M. *Chem. Lett.* **1999**, 1017.
(9) Morcrette, M.; Leriche, J. B.; Patoux, S.; Wurm, C.; Masquelier, C. *Electrochem. Solid State Lett.* **2003**, *6*, A80.
(10) Patoux, S.; Wurm, C.; Morcrette, M.; Rousse, G.; Masquelier, C. *J. Power Sources* **2003**, *119*, 278.
(11) Gaubicher, J.; Wurm, C.; Goward, G.; Masquelier, C.; Nazar, L. *Chem. Mater.* **2000**, *12*, 3240.
(12) Yin, S. C.; Grondey, H.; Strobel, P.; Huang, H.; Nazar, L. F. *J. Am. Chem. Soc.* **2003**, *125*, 326.
(13) Yin, S. C.; Grondey, H.; Strobel, P.; Anne, M.; Nazar, L. F. *J. Am. Chem. Soc.* **2003**, *125*, 10402.
(14) Jeener, J.; Meier, B. H.; Bachmann, P.; Ernst, R. R. *J. Chem. Phys.* **1979**, *71*, 4546.
(15) Xu, Z.; Stebbins, J. F. *Science* **1995**, *270*, 1332.
(16) Verhoeven, V. W. J.; de Schepper, I. M.; Nachtegaal, G.; Kentgens, A. P. M.; Kelder, E. M.; Schoonman, J.; Mulder, F. M. *Phys. Rev. Lett.* **2001**, *86*, 4314.
(17) Wang, F.; Grey, G. P. *J. Am. Chem. Soc.* **1998**, *120*, 970.
(18) Chaudhuri, S.; Wang, F.; Grey, C. P. *J. Am. Chem. Soc.* **2002**, *124*, 11746.
(19) Kim, N.; Vannier, R.-N.; Grey, C. P. *Chem. Mater.* **2005**, *17*, 1952.
(20) Cabana, J.; Dupre, N.; Rousse, G.; Grey, C. P.; Palacin, M. R. *Solid State Ionics* **2005**, *176*, 2205.
(21) Paris, M. A.; Martinez-Juarez, A.; Iglesias, J. E.; Rojo, J. M.; Sanz, J. *Chem. Mater.* **1997**, *9*, 1430.
(22) Martinez-Juarez, A.; Pecharroman, C.; Iglesias, J. E.; Rojo, J. M. *J. Phys. Chem. B* **1998**, *102*, 372.
(23) Maldonado-Manso, P.; Losilla, E. R.; Martinez-Lara, M.; Aranda, M. A. G.; Bruque, S.; Mouahid, F. E.; Zahir, M. *Chem. Mater.* **2003**, *15*, 1879.
(24) Yin, S. C.; Strobel, P. S.; Grondey, H.; Nazar, L. F. *Chem. Mater.* **2004**, *16*, 1456.
(25) Lee, Y. J.; Wang, F.; Grey, C. P. *J. Am. Chem. Soc.* **1998**, *120*, 12601.
(26) Vanmoorsel, G. J. M. P.; Vaneck, E. R. H.; Grey, C. P. *J. Magn. Reson. A* **1995**, *113*, 159.
(27) Benhabbour, S. R.; Chapman, R. P.; Scharfenberger, G.; Meyer, W. H.; Goward, G. R. *Chem. Mater.* **2005**, *17*, 1605.
(28) Bykov, A. B.; Chirkin, A. P.; Demyanets, L. N.; Doronin, S. N.; Genkina, E. A.; Ivanovshits, A. K.; Kondratyuk, I. P.; Maksimov, B. A.; Melnikov, O. K.; Muradyan, L. N.; Simonov, V. I.; Timofeeva, V. A. *Solid State Ionics* **1990**, *38*, 31.
(29) Carlier, D.; Menetrier, M.; Grey, C. P.; Delmas, C.; Ceder, G. *Phys. Rev. B* **2003**, *67*, 174103/1.
(30) Grey, C. P.; Dupre, N. *Chem. Rev.* **2004**, *104*, 4493.
(31) Gee, B.; Horne, C. R.; Cairns, E. J.; Reimer, J. A. *J. Phys. Chem. B* **1998**, *102*, 10142.
(32) Bain, A. D. *Prog. Nucl. Magn. Reson. Spectrosc.* **2003**, *43*, 63.
(33) Harris, R. K. *Nuclear Magnetic Resonance Spectroscopy: A Physicochemical View*; Pitman: London, 1983.
(34) Brown, S. P.; Spiess, H. W. *Chem. Rev.* **2001**, *101*, 4125.
(35) Bruce, P. G. *Solid State Electrochemistry*; Cambridge University Press: New York, 1995.
(36) Losilla, E. R.; Aranda, M. A. G.; Bruque, S.; Paris, M. A.; Sanz, J.; West, A. R. *Chem. Mater.* **1998**, *10*, 665.
(37) Boilot, J. P.; Collin, G.; Colomban, P. *J. Solid State Chem.* **1988**, *73*, 160.